Cost Evaluation of Two Concepts for the Integration of Hydro-pneumatic Energy Storage in Floating Wind Turbines

IOP Conf. Series: Journal of Physics: Conf. Series **1037** (2018) 042019 doi:10.1088/1742-6596/1037/4/042019

Cost Evaluation of Two Concepts for the Integration of Hydro-pneumatic Energy Storage in Floating Wind Turbines

T. Sant[1,2], D. Buhagiar[1], R. N. Farrugia[2], D. Farrugia[1] and F. M. Strati[1,2]
[1] Department of Mechanical Engineering, University of Malta, Msida MSD 2080, Malta
[2] Institute for Sustainable Energy, University of Malta, Marsaxlokk MXK 1531, Malta.

E-mail: tonio.sant@um.edu.mt

1. Introduction

As costs of offshore wind are declining, it is sensible to evaluate options for integrating large-scale energy storage to address grid management issues resulting from higher penetration of renewables. Integrating storage within the offshore turbine structure itself will reduce space requirements onshore and offer opportunities for cost reductions associated with longer and heftier power transmission cables. This is even more important for floating offshore wind turbines (FOWTs), which are being targeted for far offshore sites [1]. Energy storage technologies may be classified into four main groups: mechanical (e.g. pumped-hydro, flywheels, compressed air), thermal (e.g. sensible/latent heat storage), electro-chemical (batteries, capacitors, fuels cells) and chemical (e.g. power-to-gas, synthetic fuels). For an overview of technologies, refer to [2-4]. Pumped-hydro storage (PHS) is still the storage option with the largest capacity globally due to low cost, with efficiencies now reaching 80 % [3]. This is followed by compressed air energy storage (CAES), though this generally operates at lower round trip efficiencies (< 70 %) mainly due to the thermal losses incurred when air at atmospheric pressure is compressed to high storage pressures [4]. Both PHS and CAES have a long service life (50-100,000 cycles), but they are geographically restricted by a need for high altitude terrain or underground caverns.

Studies have shown that short-term storage that would allow intermittent power to be converted into schedulable output with short-term intervals (< 3 hours) has much greater value economically [5]. Recently, there has been increased interest in coupling wind farms to battery banks with different regulation strategies for short-term storage [6, 7]. The main contender driven by industry today are Li-Ion batteries due to the rapid decline in costs. Yet, such batteries still pose challenges related to safety (fire risks), recyclability and the supply chain, due to increased demand from relying sectors (energy, ICT, transport). Lifetime remains another challenge for integrating such batteries with wind farms given the limited storage cycles that they can offer. As shown by Barnhart *et al* [8] from Stanford University, it is more challenging to integrate storage with wind farms than with solar power given the much larger number of storage cycles required to deal with higher levels of intermittency. It should be noted that FOWTs require a long service life (25 – 30 years) to be viable, which implies that integration of PHS and CAES options should still be relevant energy storage options for the emerging floating wind market. Research into different concepts is currently being pursued to adopt PHS and CAES systems offshore. These include the Stensea and MIT ORES concepts which involve the deployment of spheres on the seabed for underwater PHS [9, 10] and energy bags which involve underwater isobaric CAES [11, 12]. A major limitation of such concepts is the high sensitivity to sea depth, with depths typically larger than 500 m often required to reach reasonable storage densities. This would make it difficult to locate such devices close to floating offshore wind turbines (FOWTs) which are being targeted for intermediate deep waters of less than 200 m.

This paper deals with hydro-pneumatic energy storage (HPES) integrated in FOWTs. HPES, which has been applied to various power engineering applications [13], combines the high energy density of CAES with the high power density of hydraulic power transmission. The basic operating

principle of an HPES system coupled to a wind turbine is explained in Figure 1. Excess energy from the wind turbine is used to power a hydraulic machine in pumping mode to inject sea water into an accumulator that is pre-charged with compressed air. During periods with low wind speeds, pressurised sea water within the accumulator is allowed to flow through the machine such that it operates in turbine mode and generates electricity, thereby maintaining a stable power output. Use of variable speed operation of the hydraulic machine allows higher conversion efficiencies to be achieved over a wider range of accumulator pressure and sea water flowrates. By appropriately sizing the accumulator it is possible to convert the intermittent wind turbine output into a stepped variation as shown in Figure 1, hence providing a scheduled, fixed power supply to the grid over a stipulated time frame.

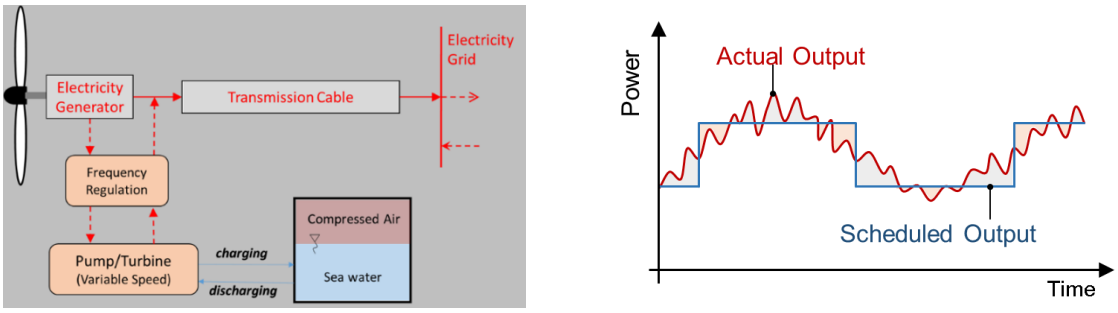

Figure 1. Operating principle of a wind turbine-integrated hydro-pneumatic energy storage concept

HPES systems at sea offer important advantages over conventional CAES systems:
(1) air is compressed using a liquid piston hydraulically, using seawater instead of pistons, thus avoiding friction and leaks;
(2) using a hydraulic pump-turbine offers a higher power density than air compressor/turbines, implying that a smaller turbomachine is required and a faster time response to fluctuations in wind power may be provided; and
(3) Submerging the accumulator in sea water and using a liquid piston with a large surface area enhances heat exchange of the air with the surrounding environment, approaching isothermal conditions. This improves the thermal efficiency of the energy storage process.

2. Objectives

This paper presents a preliminary cost evaluation of two different FOWT floating platform concepts integrating hydro-pneumatic energy storage. The analysis is based on tension leg platforms (TLPs) each supporting a 6 MW wind turbine. The two platform concepts are depicted in Figure 2. *Concept A* involves an unmodified TLP platform and HPES is integrated through a seabed-mounted accumulator. On the other hand, *Concept B* makes use of the internal volume available in the floating platform to act

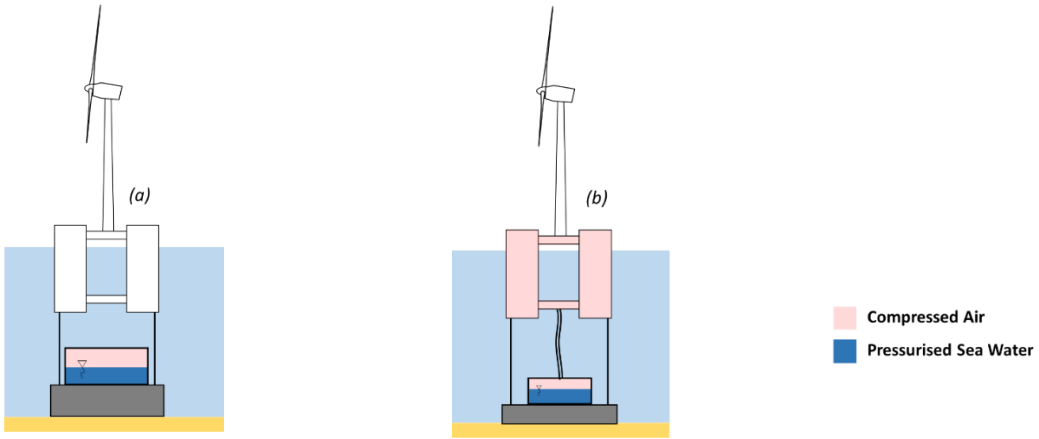

Figure 2. *Concept A* (left) and *Concept B* (right)

as a compressed air pressure vessel, apart from also providing the necessary buoyancy to keep the FOWT afloat. An accumulator is installed on the seabed and this is interconnected to the floating platform via a pneumatic umbilical.

Earlier studies related to *Concept B*, which is patent pending [14], may be found in [15,16]. In the present study it is assumed that both concepts use a concrete gravity-based foundation to anchor the TLP and energy storage accumulator. Exploiting the internal volume available in the floating platform in *Concept B* reduces the size requirements of the seabed accumulator and foundation, if compared to *Concept A*. However, this comes at the expense of having to increase the wall thickness of the platform structure to support compressed air. Furthermore, *Concept A* benefits from higher cost savings in deep waters, given that the hydrostatic pressure reduces the wall thick requirements of the accumulator. The main scope of the present work is to combine a simplified theoretical approach for sizing the TLP structures with integrated HPES systems with a cost model to compare the hardware costs of both concepts.

3. Numerical Modelling

The simplified model for sizing the floating TLPs assumes static equilibrium in still water conditions. It also assumed that the thermodynamic compression and expansion processes are purely isothermal. This condition would only be applicable if the rate at which seawater is injected into the pressure vessel is sufficiently low to allow any heat generated through the increased air pressure to be dissipated quickly to the surrounding sea water, hence keeping a constant temperature. Once the floating structure is deployed at sea, the HPES system is pressurised to an initial pre-charge pressure p_1. V_A is the volume of injected seawater in the HPES system when the system is fully charged, i.e. the maximum allowable limit of seawater in the system. V_B denotes the final volume of air in the system at fully charged conditions, with a peak air pressure p_2. The maximum energy stored and peak pressures can be expressed in terms of the pressure ratio r_p as:

$$\boldsymbol{E = p_2 V_B \ln\left(\frac{V_A + V_B}{V_B}\right) = p_2 V_B \ln(r_p)} \quad (1) \qquad \boldsymbol{p_2 = p_1\left(\frac{V_A + V_B}{V_B}\right) = p_1(r_p)} \quad (2)$$

3.1. Sizing the Floating Platform for Concepts A and Concept B

Figure 3 shows the principal dimensions defining the floating platform geometry for both concepts. Each platform is assumed to consist of a finite number *n* of cylindrical structures, each of diameter *D*. In this simplified analysis, it is also assumed that the upper and lower parts of the cylindrical floating structures are flat with a thickness equal to that of the cylindrical walls. In reality, these have to be dome-shaped to minimise build-up of material stress. Variables h_1 and h_2 denote the draft and total height of the floating structure respectively. Variable h_3 is the height of the free board section above the mean water level. The height of the concrete ballast is represented by the term h_4. The wall thickness of the cylindrical and flat surfaces of the platform in *Concept A* is denoted by t_{st}. *Concept B* has to accommodate compressed air such that the total thickness, t_{tot}, has to be larger than t_{st}. Combining thin cylinder theory for the material hoop and longitude stresses together with the von Mises' theory for elastic failure in ductile materials, it can be shown that the additional wall thickness, t_{ca}, required to support compressed air at a peak pressure p_2 is equal to:

$$\boldsymbol{t_{ca} = \frac{\sqrt{3} f_{st} D}{4}\left(\frac{p_2}{\sigma_y}\right)} \quad (3)$$

where f_{st} denotes the factor of safety based on the yield strength σ_y. For a derivation of this relation refer to [16]. The total mass of steel in each floater ($M_{st,f}$) is simply computed from:

$$\boldsymbol{M_{st,f} = \rho_{st} n \frac{\pi}{2} D t_x [D + 2h_2]} \quad (4)$$

where and $t_x = t_{st}$ for *Concept A* while $t_x = t_{tot} = t_{st} + t_{ca}$ for *Concept B*. Under purely static conditions in which no wind and waves are present, the total upthrust acting on the floating structure is equal to $\rho_{SW}V_d$. For equilibrium conditions the following relation should apply:

$$\frac{\boldsymbol{\rho_{sw}V_d}}{\boldsymbol{K}} = \boldsymbol{M_{fowt} + M_{st,f} + M_{ca} + M_b} \tag{5}$$

K is the buoyancy-to-weight ratio of the TLP. V_d is the displaced volume. M_{fowt}, M_{ca} and M_b denote the wind turbine mass (including the tower), the mass of compressed air in the platform and mass of ballast respectively. M_{ca} is determined using the ideal thermodynamic gas equation. By combining the mentioned relations it can be shown that the total floater height h_2 for *Concept B* may be expressed as:

$$\boldsymbol{h_2} = \frac{\frac{\boldsymbol{\rho_{sw}h_3}}{\boldsymbol{K}} + \frac{\boldsymbol{4\left(M_{fowt}+M_b\right)}}{\boldsymbol{n\pi D^2}} + \boldsymbol{D}\left[\frac{\sqrt{3}}{2}\left(\frac{\boldsymbol{\rho_{st}}}{\boldsymbol{\sigma_y}}\right)\boldsymbol{f_{st}p_2} + \frac{\boldsymbol{2\rho_{st}t_{st}}}{\boldsymbol{D}}\right] - \frac{\boldsymbol{p_2}}{\boldsymbol{RT}}\left(\boldsymbol{h_4}\right)}{\frac{\boldsymbol{\rho_{sw}}}{\boldsymbol{K}} - \boldsymbol{p_2}\left[\frac{\boldsymbol{1}}{\boldsymbol{RT}} + \sqrt{\boldsymbol{3}}\boldsymbol{f_{st}}\left(\frac{\boldsymbol{\rho_{st}}}{\boldsymbol{\sigma_y}}\right)\right] - \frac{\boldsymbol{4\rho_{st}t_{st}}}{\boldsymbol{D}}} \tag{6}$$

The draft h_1 can be simply computed by subtracting the freeboard height h_3 from h_2. The values for h_1 and h_2 for Concept B can still be determined using Eq. (6), however setting $p_2 = 0$. This model assumes that the buoyancy and the internal volume offered by any secondary members interconnecting the vertical cylindrical structures of the floaters are ignored.

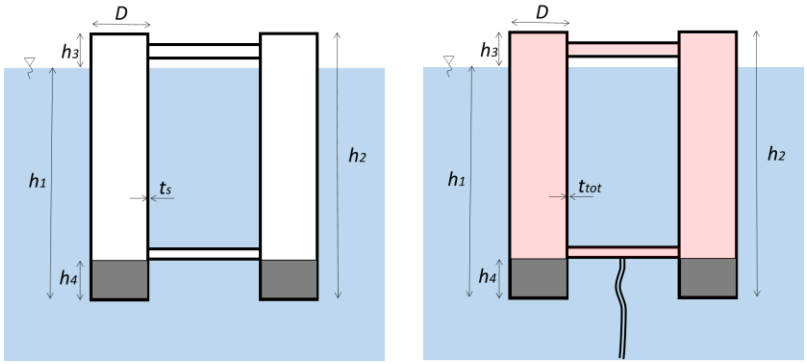

Figure 3. Principal dimensions for platform of *Concept A* (left) and *Concept B* (right)

3.2. Sizing the Seabed Accumulators for Concept A and Concept B

The sea-bottom structure for both *Concepts A* and *B* is modelled as a set of n_l horizontal steel pressure vessels making up the accumulator and assembled on a steel-reinforced concrete gravity foundation. All vessels have the same diameter equal to that of the floater cylindrical structures D. The ends of the pressure vessels are also assumed to be flat, with the thickness equal to that of the cylindrical walls. This thickness is computed using Eq. (3), however this is modified to replace the peak CAES pressure p_2 by $(\boldsymbol{p_2 - \rho_{sw}gH})$, to allow for the higher hydrostatic pressure of seawater at a sea depth H. This caters for smaller wall thickness requirements of pressure vessels installed in deeper waters. The concrete foundation is sized to balance the tension from the TLP tethers (equal to $\boldsymbol{\rho_{sw}gV_d\left(1 - K^{-1}\right)}$), as well as the upthrust due to the presence of the sea-bottom pressure vessels and the foundation itself. A factor of safety is included by increasing the total mass of the concrete foundation by a factor f_c. It should be noted that the concrete foundation is determined for a worst case scenario at which V_A is zero, hence maximum upthrust is acting of the seabed structure.

3.3. Cost Model

The cost model presented in this study only considers the hardware costs, including (1) steel material and fabrication for both the floating platform and seabed accumulator; (2) steel-reinforced concrete for

ballasting and the gravity foundation; (3) TLP tethers and a pneumatic umbilical; (4) the pump-turbine; (5) painting and corrosion protection components and (6) auxiliary systems. Costs related to the overall system assembly, transportation, installation and eventual decommissioning at the offshore site are not included. The cost of steel is expressed through the following relation:

$$\boldsymbol{C_{st} = \left[c_{st,mat} \times \left(M_{st,f} + M_{st,sb}\right)\right] + \left[c_{st,fab}(t_x) \times M_{st,f}\right] + \left[c_{st,fab}(t_x) \times M_{st,sb}\right]} \quad (7)$$

where $M_{st,sb}$ is the mass of steel used for the seabed structure. $c_{st,mat}$ is the material cost of steel in Euro/kg and $c_{st,fab}(t_x)$ is the fabrication cost of steel in Euro/kg expressed as a function of steel sheet thickness. It is expected that economies of scale enable cost reductions in fabrication processes involving cutting, rolling and automated welding, leading the fabrication costs per unit mass to decrease for thicker steel sheets. In the present model, it is assumed that the fabrication cost decreases linearly with plate thickness in accordance with the relation:

$$\boldsymbol{c_{st,f}(t_x) = c_{st,f} + \frac{(t_x - 200)}{(10 - 200)} \times \left(c_{st,f,10} - c_{st,f,200}\right)} \quad (8)$$

where t_x is the sheet thickness expressed in mm and $c_{st,f,\,10}$ and $c_{st,f,200}$ denote that fabrication costs for steel sheets having a thickness of 10 and 200 mm, respectively. Concrete costs are simply expressed in terms of Euro per cubic metre:

$$\boldsymbol{C_c = c_c \times \left[V_{c,b} + V_{c,fnd}\right]} \quad (9)$$

where $V_{c,b}$ and $V_{c,fnd}$ denote the volume of concrete used for TLP ballasting and the sea-bottom gravity foundation. c_c is the cost of steel-reinforced concrete per unit volume. The cost for the TLP taut mooring is assumed to increased linearly with the product of the length and tension being sustained, as follows:

$$\boldsymbol{C_{mr} = n_t \times c_{mr} \times (H - h_1)} \quad (10)$$

where n_t is the number of tethers in tension while c_{mr} is the cost of the mooring per newton-metre. The above formulation allows for higher tether costs as the tension requirements increase. It is assumed that the TLP moorings extend from the base of the floater cylindrical structures down to the gravity foundation located at the seabed. The cost of the pneumatic umbilical for *Concept B* is expressed using the following relation:

$$\boldsymbol{C_{pu} = c_{pu} \times (H - h_1) \times f_{pu}} \quad (11)$$

C_{pu} is the cost of the umbilical per unit length in Euro/m and H is the sea depth. The term f_{pu} is a safety factor applied to the minimal length ($H - h_1$) to ensure that the umbilical is freely buoyant and does not become taut while the TLP is surging. Painting costs are determined in terms of Euro per metre squared of surface area. It is assumed that the floater and sea-bottom steel cylindrical structures are painted on both the exterior and interior surfaces. The pump turbine cost is expressed as:

$$\boldsymbol{C_{pt} = c_{pt} \times P_r} \quad (12)$$

where c_{pt} is the specific cost in terms of Euro/kW and P_r is the rated capacity. The overall cost, C_{tot} of the entire floating support structure with integrated HPES is equal to the total sum of different costs, with factors to account for engineering design and management costs as well as overall profits such that:

$$\boldsymbol{C_{tot} = \left(C_{st} + C_c + C_{mr} + C_{pu} + C_{pnt} + C_{corr} + C_{pt} + C_{an}\right) \times \left(1 + \frac{k_{edm}}{100}\right)\left(1 + \frac{k_{prf}}{100}\right)} \quad (13)$$

where C_{pnt}, C_{corr} and C_{an} are the costs of painting, corrosion protection devices and ancillary platform systems. k_{edm} is the percentage cost related to engineering design and management costs and k_{prf} is the

percentage profit made in developing the structure. C_{tot} only considers hardware related to the TLP structure with integrated HPES. Costs related to the wind turbine and electrical cabling are excluded.

4. Requirements for Energy Storage and Pump-Turbine Capacity

Open source wind measurements for typical North Sea meteorological conditions were obtained from the Egmond aan Zee wind farm in the Netherlands [17]. A dataset of 10 minute-average wind speed measurements over the period July 2005 to June 2006 was used to determine the energy storage capacity requirements to transform the intermittent power output from a 6 MW wind turbine into a scheduled stepped output at different intervals (Fig. 1). Table 1 shows the storage capacity required to maintain the power supply constant over 1, 2 and 3-hour intervals. It is shown that over a target FOWT lifetime of 30 years, the number of cycles handled by the concept system is significantly larger than that of batteries working with electro-chemical storage, which in most cases have a lifetime in the range of only 500 – 10,000 cycles [18]. One cycle denotes a change between storage system charging and discharging modes. It is observed that the number of cycles based on the 10 min data is significantly lower than the fatigue cycles typically encountered by wind turbines over their lifetime. Table 1 also shows the pump-turbine rating required to be able to manage the different stepped-output intervals. It should be noted that these estimates ignore losses incurred during the energy storage processes. Consequently, figures for the required storage capacity are conservative.

Table 1. Requirements for storage capacity, cycles and pump-turbine capacity

Scheduling Period	Storage Capacity	Storage Cycles over 30 years	Pump-Turbine Rating
1 Hour	1.6 MWh	197,700	1.8 MW
2 Hours	3.8 MWh	138, 60	1.9 MW
3 Hours	7.5 MWh	94,110	2.0 MW

5. Parametric Analysis for Concepts Designs

A parametric analysis was carried out to investigate the influence of critical design parameters on the overall hardware cost C_{tot} (Eqt. 13) of floating TLP platforms integrating *Concepts A* and *B* (Fig. 2). The TLP platforms are assumed to support a 6 MW horizontal-axis wind turbine, with the mass indicated in Table 2. Unless otherwise indicated in the plotted results (Figs. 4 – 10), the values of parameters retained fixed during the analysis are as shown in Tables 2 to 7. For all simulated design configuration, the concrete ballast was adjusted for both TLP variants such that the resulting displacement and draft of both platforms would be equal.

Table 2. Wind Turbine Parameters

Rotor mass	170 tonnes
Nacelle mass	240 tonnes
Tower	372 tonnes
Total wind turbine mass (M_{fowt})	782 tonnes

Table 3. Design Parameters for Floating Platform

Concept	A	B	Concept	A	B
Number of vertical cylindrical structures (n)	4	4	Freeboard height (h_3)	10 m	10 m
Diameter of vertical cylindrical structures (D)	6 m	6 m	Draft (h_2)	46.6 m	46.6 m
Buoyancy-to-weight ratio (K)	1.3	1.3	Volumetric displacement (V_d)	5265 m^3	5265 m^3
Number of TLP tethers (n_t)	4	4	Concrete ballast mass (M_b)	2841 t	430 t

Table 4. Design Parameters for Seabed Structure

Concept	A	B
Number of horizontal pressure vessels (n_l)	8	4
Diameter of horizontal pressure vessels (D)	6 m	6 m
Length of horizontal pressure vessels (L_l)	56.7 m	58.4 m
Total sea bed accumulator volume (V_l)	12,820 m^3	6,600 m^3

Table 5. Design Parameters for HPES

Compressed air temperature (T)	4
Characteristic gas constant (R)	6 m
Peak compressed air pressure (p_2)	60 Bar
Energy storage capacity (E)	7.5 MWh
Pump-turbine rated power (P_r)	2 MW

Table 6. Parameters for steel and concrete

Density of steel (ρ_{st})	7850 kg/m^3
Yield strength for steel (σ_y)	475 N/mm^2
Factor of safety for steel (f_{st})	1.7
Density of steel-reinforced concrete (ρ_c)	2450 kg/m^3
Factor of safety on concrete gravity foundation (f_c)	1.5

Table 7. Cost Parameters

Steel raw material ($c_{st,mat}$)	€ 0.6/kg	Density of steel-reinforced concrete (r_c)	2450 kg/m^3
Steel manufacturing costs for 10mm thickness ($c_{st,fab,10}$)	€ 1.5/kg	Factor of safety on concrete gravity foundation (f_c)	1.5
Steel manufacturing costs for 200mm thickness ($c_{st,fab,200}$)	€ 1.5/kg	Painting	€ 60 /m^2
Steel-reinforced concrete (c_c)	€ 230/m^3	Corrosion protection devices (C_{corr})	€ 20,000
Mooring lines (c_{mr})	€ 2783 /Nm	Ancillary platform systems	€ 500,000
Pump-turbine (c_{pt})	€ 500 /MW	Engineering design & management (k_{edm})	2.5 %
Pneumatic umbilical (c_{pu})	€ 500 /m	Profit (k_{prf})	2.5 %

A fixed sea depth of 150 m is assumed throughout the study, unless otherwise specified. Based on the parameters presented in Table 2 to 6, it is estimated that 87 MWh would be initially required following deployment to pre-charge the HPES system in both concepts to the initial pressure p_1. This estimate is based on an auxiliary air compressor efficiency of 40%. The estimate amounts to < 0.5% of the wind turbine yield for one year for a site having a wind turbine capacity factor of 45%. The overall hardware cost (C_{tot}) is primarily dominated by the costs of steel, concrete, the pump-turbine and the mooring lines. The assumed price of steel plate is within the price range of hot rolled sheets observed in 2017 [19]. The price of steel-reinforced concrete typically varies between Euro 100 – 650/m^3. The price is significantly dependent on the concrete grade and the type of steel re-enforcement being integrated in the casting, with the cost increasing rapidly as the mass and complexity of the steel re-enforcement is increased. A value of Euro 250/t, equivalent to Euro 614/m^3, was assumed in the Innwind project [20] for floating wind turbine applications which would demand significant steel re-enforcement to support the large cyclic stresses encountered by the floating support structure. A significantly lower value (Table 7) is assumed in this study as the concrete is only being intended for ballasting and the gravity foundation. The cost of a pump-turbine was based on typical costs for pumped hydro turbines [21]. The cost coefficient for the mooring lines (c_{mr}) was derived based on cost data presented for a TLP in the Pelastar concept [22]

5.1. Influence of Sea-bottom Accumulator Capacity

Figures 4 and 5 illustrate the influence of increasing the sea water volumetric capacity of the seabed mounted accumulator (V_A) on the energy storage characteristics of *Concepts A* and *B*. It is observed that increasing this capacity reduces the cost of storage for both systems, with the expense of having to operate at a higher pressure ratio (r_p). This would increase thermal losses due to higher peak temperatures induced by the air compression process. Yet this is still significantly lower than that of conventional CAES systems (operating at typically $r_p > 20$). It is observed in Figure 4 that the cost of a platform implementing *Concept B* is consistently lower than that of *Concept A*. This is primarily due to the significantly smaller seabed structure (Fig. 5), which would reduce the overall hardware costs. In reality, the smaller structure would also be expected to decrease installation costs, however these are not being accounted for in this study.

5.2. Influence of TLP Buoyancy-to-Weight Ratio

Larger values for the design buoyancy-to-weight ratio (K) result in higher costs in terms of Euro/kWh (Fig. 6) as a result of the larger buoyancy requirements to support a given floating structure mass. However, the sensitivity to variations in K is larger for *Concept B* than *Concept A*, with the resulting effect being that the cost ratio (*Concept B*/*Concept A*) decreases at larger buoyancy-to-weight ratios. It may be noted that large values of K would also increase the storage capacity and reduced the peak pressure ratio (r_p) (Fig. 7). Yet, these variations are only marginal (< 4%). Results in Fig. 7 are common to both concepts, given that the pressure ratio and volumetric values V_A and V_B are retained equal.

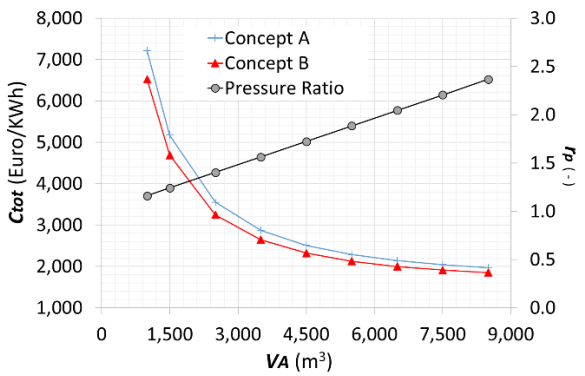

Figure 4. Variation of Platform Cost and Pressure Ratio with Seabed Accumulator Capacity

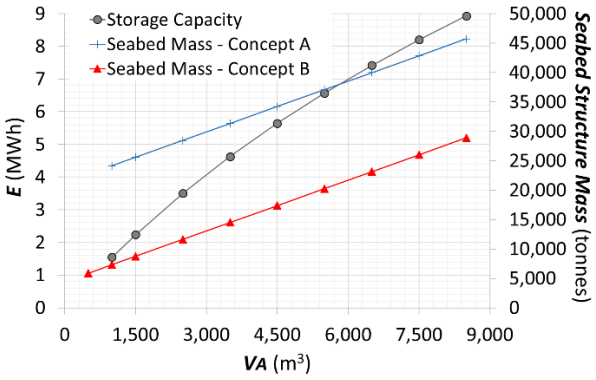

Figure 5. Variation of Storage Capacity and Seabed Structure Mass with Seabed Accumulator Capacity

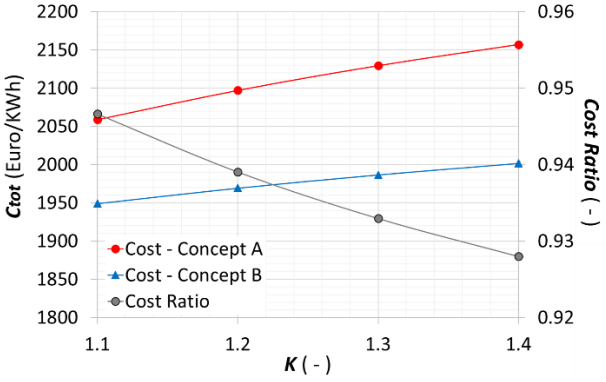

Figure 6. Variation of Platform Cost and Cost Ratio with Buoyancy-to-Weight Ratio

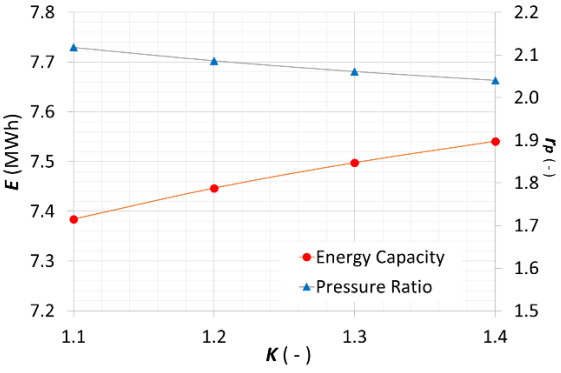

Figure 7. Variation of Storage Capacity and Pressure Ratio with Buoyancy-to-Weight Ratio

5.3. Influence of the Rated Peak Operating Pressure

The influence of the peak compressed air pressure is depicted in Fig. 8 and 9. Lower costs and higher storage capacities may be achieved when designing for higher values of p_2, with *Concept B* remaining the cheaper option for the 150 m sea depth being considered here. As may be noted from Fig. 9, higher design peak pressures reduce marginally the pressure ratio. The wall thickness of the floating platform in *Concept B* increases linearly with p_2, in accordance with Eq (3). One the other hand, the thickness of material used in *Concept A* would remain unchanged, given that no compressed air is present in the platform.

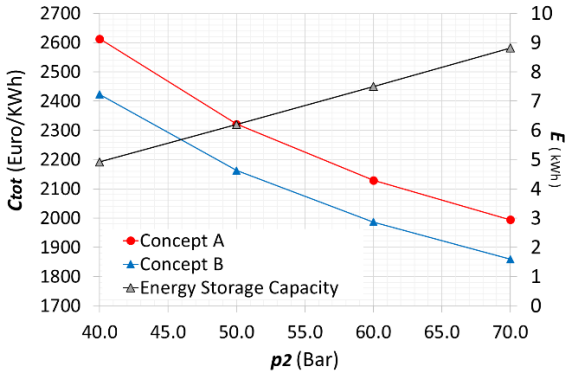

Figure 8. Variation of Platform Cost and Storage Capacity with Peak Air Pressure

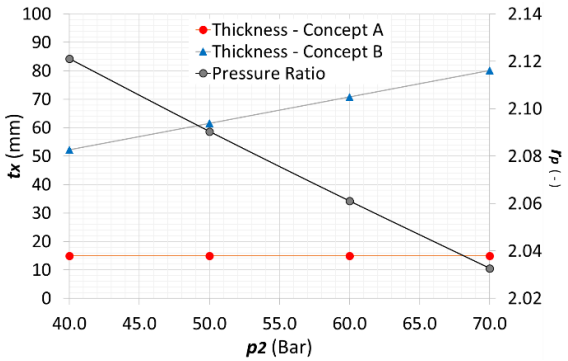

Figure 9. Variation of Platform Wall Thickness and Pressure Ratio with Peak Air Pressure

5.4. Influence of Sea Depth and Steel Fabrication Costs

The variation of cost ratio with sea depth is plotted in Fig. 10. This ratio is shown to be less than unity, implying that *Concept B* would be a less expensive option for the sea depth considered. The cost advantage however decreases with depth, and *Concept A* would be expected to involve lower hardware costs in deep waters. The cost ratio shown in Fig. 10 is plotted for different values of $C_{st,f,200}$ (Eq (8)). The latter parameter accounts for lower steel fabrication costs when rolling and welding thicker steel sheets. With $C_{st,f,200}$ =1.5 kg, cost reductions attributed to fabrication of thicker sheets is not accounted for. At the lowest considered value of $C_{st,f,200}$ = Euro 0.5/kg, fabrication costs for a cylindrical structure with a wall thickness of 70 mm would cost Euro 1.18/kg instead of Euro 1.5/kg.

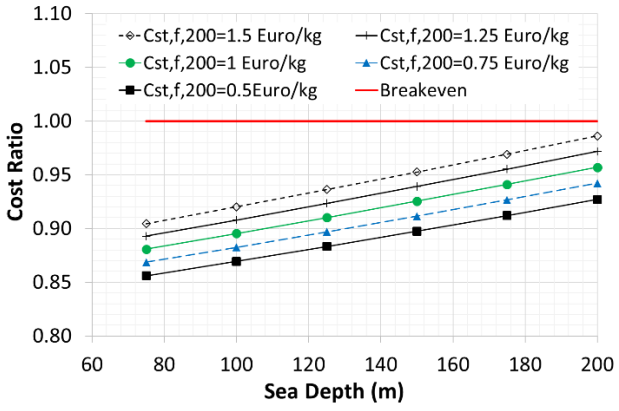

Figure 10. Variation of floating platform costs and cost ratio (*Concept B/Concept A*) with depth.

6. Conclusions

This study has shown that integrating HPES within TLP structures for floating wind turbines using the support structure itself as a compressed air vessel that is pneumatically linked to an accumulator on the seabed may be a more viable option for intermediate deep waters than having only a large accumulator on the seabed, with the TLP floating structure kept unaltered. This provides motivation for conducting more detailed numerical studies involving fully coupled aero-hydro-structural simulations to optimise

the TLP design for HPES integration using the former option, taking into account structural stability and fatigue load minimisation as well as the energy efficiency of the HPES process.

7. References

[1] Hundleby, G. and Freeman, K., *Unleashing Europe's offshore wind potential - A new resource assessment*, BVG Associates, June 2017.
[2] Aneke, M. and Wang, M., *Energy Storage Technologies and Real Life Applications – A State of the Art Review*, Applied Energy 179, 2016, pp. 350-77.
[3] Sabihuddin, S., Kiprakis, A.E. and Mueller, M., *A Numerical and Graphical Review of Energy Storage Technologies*, Energies 8.1, 2014, pp. 172-216.
[4] Sánchez Muñoz, A., Garcia, M. and Gerlich, M., *Overview of storage technologies*, report from H2020 funded project SENSIBLE, Grant Agreement No. 645963, December 2016.
[5] Staffell, I. and Rustomji, M., *Maximising the value of electricity storage*, Journal of Energy Storage, 8, 2016, pp. 212–225.
[6] Abdullah, M.A., Muttaqi, K.M., Sutanto, D. and Agalgaonkar, A.P., *An Effective Power Dispatch Control Strategy to Improve Generation Schedulability and Supply Reliability of a Wind Farm Using a Battery Energy Storage System*, IEEE Transactions on Sustainable Energy, Vol. 6, (3), July 2015.
[7] Zhang, X., Yuan, Y., Hua, L., Cao, Y. and Qian, K., *On Generation Schedule Tracking of Wind Farms with Battery Energy Storage Systems*, IEEE Transactions on Sustainable Energy, Vol. 8, No. 1, January 2017.
[8] Barnhart, C.J., Dale, M., Adam, R., Brandt, A.R. and Bensonab, S.M., *The energetic implications of curtailing versus storing solar- and wind-generated electricity*, Environ. Sci., 6, 2804, 2013, DOI: 10.1039/c3ee41973h.
[9] Hahn, H., Hau, D., Dick, D. and Puchta, M., *Techno-economic assessment of a subsea energy storage technology for power balancing services*, Energy, 133, 2017, pp. 121-127.
[10] Slocum, A.H., Fennell, G.E., Dundar, G., Hodder, B.G., Meredith, J.D.C. and Sager, M.A., *Ocean Renewable Energy Storage (ORES) System: Analysis of an Undersea Energy Storage Concept*, Proceedings of the IEEE, Vol. 101, (4), April 2013.
[11] Pimm A.J., Garvey S.D. and de Jong, M., *Design and testing of Energy Bags for underwater compressed air energy storage*, Energy, Vol. 66, 1 March 2014, pp. 496-508.
[12] Cheung B.C., Carriveau, R. and Ting, D., *Parameters affecting scalable underwater compressed air energy storage*, Applied Energy, Vol. 134, December 2014, pp. 239-247.
[13] Cronk, P.M. and Van de Ven, D., *A review of hydro-pneumatic and flywheel energy storage for hydraulic systems*, International Journal of Fluid Power, 2017, DOI:10.1080/14399776.2017.1386061
[14] Sant, T. and Buhagiar, D., *Hydro-pneumatic energy storage system*, Patent WO2016128962 A1, August 2016.
[15] Buhagiar, D. and Sant, T., *Modelling of A Novel Hydro-Pneumatic Accumulator For Large-Scale Offshore Energy Storage Applications*, Journal of Energy Storage, Elsevier - Special Issue – Vol. 14, Part 2, December 2017, https://doi.org/10.1016/j.est.2017.05.005
[16] Sant, T. Buhagiar, D. and Farrugia, R.N., *Modelling the Dynamic Response and Loads of Floating Offshore Wind Turbine Structures with Integrated Compressed Air Energy Storage*, OMAE2017-61587, ASME 36th Conference on Ocean, Offshore and Arctic Engineering, June 25-30, 2017, Trondheim, Norway.
[17] www.noordzeewind.nl/en/project-en/; Accessed August 2017.
[18] International Renewable Energy Agency (IRENA), Electric*ity Storage and Renewables – Costs and Markets to 2030*, October 2017.
[19] http://www.meps.co.uk/world-price.htm, Accessed January 2018
[20] InnWind.EU, Deliverable D4.3.3 – *Innovative Concepts for Floating Structures*, August 2014, http://www.innwind.eu, Accessed September 2017.

[21] International Renewable Energy Agency (IRENA), *Renewable Energy Technologies: Cost Analysis Series, Vol.1 Hydropower*, June 2012.
[22] Hurley, W.L, and Nordstrom, C.J., *Pelastar Cost of Energy: A cost study of the Pelastar floating foundation system in UK waters*, report prepared for the Energy Technologies Institute, UK, January 2014.

Acknowledgments
This work is part of the Project FLASC (R&I-2015-044-T) being carried out with the industrial partner Medserv p.l.c. and supported by the Malta Council for Science & Technology through the FUSION R&I Technology Development Programme. The project is also supported by Malta Marittima and the Research and Innovation Development Trust (RIDT) of the University of Malta. The authors would also like to acknowledge the use of the open source wind measurements from the Egmond aan Zee wind farm.